# PERFORMANCE COMPARISON OF THREE RECENT STAP METHODS

*Freeman C. Lin*[1] *and Muralidhar Rangaswamy*[2]

[1]ARCON Corporation, 260 Bear Hill Road, Waltham, MA
[2]AFRL/SNHE Hanscom Air Force Base, MA

## ABSTRACT

In this paper, we present a comparison of target detection performance for normalized adaptive matched filter (NAMF), normalized parametric adaptive matched filter (NPAMF), and normalized low-rank adaptive matched filter (LRNAMF) for space-time adaptive processing. Test statistics for these algorithms as functions of range bins and filter outputs as functions of Doppler beam position ($DBP$) and azimuth angle ($AZ$) are computed for the KASSPER L-band datacube, which is simulated for the airborne linear phased array radar application. First, we illustrate that when the signal-to-noise ratio is used as a target-detection parameter, LRNAMF outperforms NAMF and NPAMF under weak conditions of training data contamination. Next, we demonstrate the target cancellation effect when the training data are contaminated by competing targets (outliers). Finally, we present a scenario for target detection in heterogenous radar clutter when there is spatio-temporal steering vector uncertainty. In this scenario, we show that there is substantial broadening in the filter outputs as functions of $DBP$ and $AZ$ for these algorithms.

## 1. INTRODUCTION

Space-time adaptive processing (STAP) [1-5] exhibits potential benefit for target detection in airborne and space-based radars. In practice, STAP is plagued by system errors, internal clutter motion, and shadowing effects as well as non-stationary clutter scenarios. Important STAP issues include the computational cost, sample support, constant false alarm rate (CFAR), and robustness to mismatch (e.g., misalignment of the steering vector for the desired target and the range-dependent covariance matrix). According to the "Reed-Mallet-Brennan rule" [6], $K = 2JN$ training data vectors, ($J$ is the number of elements in the linear phased array and $N$ the number of pulses per element), are needed for the computation of covariance matrix and weight vector so that the signal-to-interference-and-noise ratio ($SINR$) is within 3dB of the optimum. When the problem of dimensionality (or the spatio-temporal product, $JN$) increases, the required training support, $K$, increases significantly. This imposes onerous requirements on training data collection in practice. Additionally, the computational cost grows exponentially when $JN$ increases. Moreover, since only one realization of spatio-temporal datacube is available in practice, training data need to be selected from other range bins adjacent to a test range bin, namely, a cell under test, (CUT). Over the entire radar range if the data is homogeneous, it ensures that the selected training data is representative of clutter for a CUT. However, heterogeneous clutter results in large variations over range. This spatial clutter variation imposes severe restrictions on the size of available training data. Therefore, it is a challenging research topic to devise adaptive space-time processors for target detection in heterogeneous radar clutter.

In the past, many reduced-dimension processing algorithms (e.g., selected references including [7, 8, 9, 5]) have been developed to address the problem of limited training data and to reduce the computational complexity. As mentioned by Rangaswamy [10] (and cited references therein), in many cases, the interference covariance matrix may be approximated by its low rank version. The probability of false alarm rate ($P_{\mathsf{fa}}$) and the probability of detection ($P_{\mathsf{d}}$) for the normalized low-rank matched filter (LRNMF) have been derived by Rangaswamy [10]. This work illustrates that the reduced-dimension processing produces a test statistic with robust performance with respect to unknown clutter scaling and unknown background noise level. For radar target detection in heterogeneous clutter, Monte Carlo simulations [11] have also been conducted to demonstrate that not only LRNAMF reduces the computational complexity of fully adaptive STAP but also provides a way to determine the correct clutter rank through the $P_{\mathsf{d}}$ performance. In this paper, we study the target detection performance of LRNAMF and compare it with two other methods, i.e., normalized adaptive matched filter (NAMF) [12] and normalized parametric adaptive matched filter (NPAMF) [13]. Performance analysis is carried out by Monte Carlo simulation. It is illustrated that LRNAMF can outperform NAMF and NPAMF when there are few outliers in the training data.

In Section 2, cutoff signal-to-noise ratios as functions of the sample support for NAMF, NPAMF, and LNRAMF are presented. On the other hand, performance comparisons for NAMF, NPAMF, and LRNAMF are shown in the later sec-

0-7803-8882-8/05/$20.00 (C) 2005 IEEE

# Report Documentation Page

*Form Approved*
*OMB No. 0704-0188*



| 1. REPORT DATE | 2. REPORT TYPE | 3. DATES COVERED |
|---|---|---|
| **01 MAY 2005** | **N/A** | **-** |

| 4. TITLE AND SUBTITLE | 5a. CONTRACT NUMBER |
|---|---|
| **Performance Comparison Of Three Recent Stap Methods** | 5b. GRANT NUMBER |
| | 5c. PROGRAM ELEMENT NUMBER |
| 6. AUTHOR(S) | 5d. PROJECT NUMBER |
| | 5e. TASK NUMBER |
| | 5f. WORK UNIT NUMBER |
| 7. PERFORMING ORGANIZATION NAME(S) AND ADDRESS(ES) **ARCON Corporation, 260 Bear Hill Road, Waltham, MA** | 8. PERFORMING ORGANIZATION REPORT NUMBER |
| 9. SPONSORING/MONITORING AGENCY NAME(S) AND ADDRESS(ES) | 10. SPONSOR/MONITOR'S ACRONYM(S) |
| | 11. SPONSOR/MONITOR'S REPORT NUMBER(S) |

12. DISTRIBUTION/AVAILABILITY STATEMENT
**Approved for public release, distribution unlimited**

13. SUPPLEMENTARY NOTES
**See also ADM002017. Proceedings of the 2005 IEEE International Radar Conference Record Held in Arlington, Virginia on May 9-12, 2005. U.S. Government or Federal Purpose Rights License**

14. ABSTRACT

15. SUBJECT TERMS

| 16. SECURITY CLASSIFICATION OF: | | | 17. LIMITATION OF ABSTRACT | 18. NUMBER OF PAGES | 19a. NAME OF RESPONSIBLE PERSON |
|---|---|---|---|---|---|
| a. REPORT | b. ABSTRACT | c. THIS PAGE | | | |
| **unclassified** | **unclassified** | **unclassified** | **UU** | **8** | |

**Standard Form 298 (Rev. 8-98)**
Prescribed by ANSI Std Z39-18

tion, where we present two sets of simulations to illustrate the steering-vector matched and mismatched cases as well as the target cancellation effect. In Case 1 of Section 3, simulations are performed for the case that we have the *a priori* information regarding true steering vector. Broadenings of filter output due to the steering-vector uncertainty is demonstrated in Case 2 of Section 3. Conclusions are presented in Section 4.

## 2. CUTOFF SIGNAL-TO-NOISE RATIOS

For STAP, each of $J$ array elements of the side-looking linear phased array radar transmits and receives $N$ pulses in a coherent processing interval (CPI). The measured $JN \times 1$ spatio-temporal data vector, $\mathbf{x}$, has the concatenated representation, $\mathbf{x} = [\mathbf{x}^{\mathsf{T}}(0)\mathbf{x}^{\mathsf{T}}(1)\ldots\mathbf{x}^{\mathsf{T}}(N-1)]^{\mathsf{T}}$ where $x(n)$ is a complex row vector with $J$ elements. In the binary detection problem, two hypotheses are defined as

$$\mathbf{H}_0 : \mathbf{x}(n) = \mathbf{d}(n) \quad (1)$$

$$\mathbf{H}_1 : \mathbf{x}(n) = a\mathbf{e}(n) + \mathbf{d}(n) \quad (2)$$

where $n = 0, 1, ..., N-1$. Under the hypothesis $\mathbf{H}_0$, the data vector $\mathbf{x}$ contains only the unwanted disturbance $\mathbf{d}$ with a positive definite covariance matrix $\mathbf{R}_d$ of dimension $JN \times JN$, while under the hypothesis $\mathbf{H}_1$, $\mathbf{x}$ may contain the desired target with known target steering vector $\mathbf{e}(n)$ but unknown complex amplitude $a$. The disturbance $\mathbf{d}$ may consist of the Gaussian clutter vector having a covariance matrix $q\mathbf{R}_c$ with known structure and unknown power level $q$ and the additive white Gaussian noise having the covariance matrix $\sigma^2\mathbf{I}$, where $\mathbf{I}$ is $JN \times JN$ identity matrix and $\sigma^2$ is the unknown noise power. In this case, the disturbance covariance matrix $\mathbf{R}_d$ is given by $\mathbf{R}_d = q\mathbf{R}_c + \sigma^2\mathbf{I}$. For the binary detection problem, a scalar test statistic, $\Lambda$, is computed from the array output sequence for each pulse in the CPI and compared with a specified threshold, $\lambda$. Given a single realization of $\mathbf{x}$, the hypothesis $\mathbf{H}_0 : a = 0$ is selected if $\Lambda < \lambda$ while $\mathbf{H}_1 : a \neq 0$ is declared if $\Lambda > \lambda$. In adaptive signal processing, the disturbance covariance matrix $(\mathbf{R}_d)$ needs to be computed from training data so that test statistics for NAMF, NPAMF, and LNRAMF, i.e., $\Lambda_{NAMF}$, $\Lambda_{NPAMF}$, and $\Lambda_{LNRAMF}$ can be expressed as

$$\Lambda_{NAMF} = \frac{|\mathbf{e}^H \hat{\mathbf{R}}_d^{-1}\mathbf{x}|^2}{[\mathbf{e}^H \hat{\mathbf{R}}_d^{-1}\mathbf{e}][\mathbf{x}^H \hat{\mathbf{R}}_d^{-1}\mathbf{x}]} \quad (3)$$

$$\Lambda_{NPAMF} = \frac{|\sum_{n=0}^{N-P-1} \mathbf{s}^H(n)\nu(n)|^2}{[\sum_{n=0}^{N-P-1} \mathbf{s}^H(n)\mathbf{s}(n)][\sum_{n=0}^{N-P-1} \nu^H(n)\nu(n)]} \quad (4)$$

$$\Lambda_{LRNAMF} = \frac{|\mathbf{e}^H(\mathbf{I}-\hat{\mathbf{P}})\mathbf{x}|^2}{[\mathbf{e}^H(\mathbf{I}-\hat{\mathbf{P}})\mathbf{e}][\mathbf{x}^H(\mathbf{I}-\hat{\mathbf{P}})\mathbf{x}]} \quad (5)$$

where $\hat{\mathbf{R}}_d$ is the estimated disturbance covariance matrix and the spatio-temporal steering vector, $\mathbf{e}$, is assumed to be the same as the target steering vector. Note that in Eq. (5), $\Lambda_{LRNAMF}$ is independent of the unknown noise power $\sigma^2$ and it allows two important interpretations as normalized adaptive matched filtering in the sub-dominant disturbance subspace or a dominant mode rejector followed by quadratic normalization. For NPAMF [9], $\nu$ and $\mathbf{s}$, with the reduced dimension of $J(N-P)$, are residual sequences for the spatio-temporally whitened primary data and steering vector, respectively. For LRNAMF [11], $\mathbf{I}$ and $\hat{\mathbf{P}}$ are the identity matrix and the estimated projection matrix, respectively. $\hat{\mathbf{P}}$ has a rank $r$ and is formed from the eigenvectors corresponding to the $r$ dominant eigenvalues of $\hat{\mathbf{R}}_d$. For an airborne linear phased array radar under ideal conditions the Brennan rule [5] predicts the clutter rank as:

$$r = J + \beta(N-1) \quad (6)$$

$$\beta = 2v_pT/d \quad (7)$$

where $\beta$ is the slope of the clutter ridge, $v_p$ the platform velocity, $T$ the pulse repetition interval, and $d$ the inter-element spacing. When $\beta$ has a nominal value of unity, the clutter rank $r$ is much less than the spatio-temporal product $JN$ especially with increasing $J$ and $N$. This ensures the necessity for the application of low rank approximation (5) in order to reduce the computational cost for large dimensional STAP problem and to preserve invariance with respect to the unknown clutter power and noise level.

Adaptive signal processing requires training data for estimating the disturbance covariance matrix $\hat{\mathbf{R}}_d$. It is known that if there are outliers in training data, it will cause target cancellation so that it is unable to obtain a good estimate of the threshold for further computation of test statistics. Hence, we utilize those true clutter covariance matrices for the simulated KASSPER L-band radar clutter [14] to generate the datacube containing only radar return from clutter. This set of clutter-only datacube will be used as the training data to compute $(\hat{\mathbf{R}}_d)$ for NAMF, the projection matrix $(\hat{\mathbf{P}})$ for LRNAMF [10], and the multichannel linear autoregressive coefficients for NPAMF [9]. Parameters for the simulated KASSPER L-band datacube are given in Table 1. Note that the $DBP$ is the normalized Doppler frequency with respect to the pulse repetition frequency, $T^{-1}$. This clutter-only datacube contains 1000 range bins ($RB$s) and each $RB$ consists of data matrix simulated for the linear phased array with eleven channels ($J = 11$) and thirty-two pulses ($N = 32$). In this case, the slope of the clutter ridge $\beta$ is about 0.9231 so that the Brennan's rule yields the clutter rank to be $r = J + \beta(N-1) \approx 40$. For the ideal linear phased array radar, $\beta = 1$ so that $r = 42$. Since the clutter rank for the KASSPER L-band clutter is much smaller than the spatio-temporal product $JN = 352$, the LRNAMF algorithm reduces the computational complexity and results a better target detection performance for STAP. The clutter-to-noise ratio $(CNR)$ for the simulated KASSPER L-band datacube is 40dB. The cutoff signal-to-noise ratios ($SNR$) is defined as the minimum ratio of the target to noise power so that multiple targets can be detected

simultaneously with a specified, maximum threshold. For this simulation, the cutoff $SNR$ versus sample support $K$ for NAMF, NPAMF, and LRNAMF are plotted in Figure 1. Under the sliding window processing (SWP), each half of outlier-free training data with sample support $K$ is selected symmetrically from either side of the CUT. The primary data is generated by manually inserting three targets into the clutter-only datacube at $RB = 493$, 500, and 507, respectively. These three targets have identical Doppler beam position, $DBP_T = -0.2323$, and azimuth angle, $AZ_T = 149^o$, but with various $SNR$s. In order to expedite the computation for $\Lambda_{NAMF}$, $\Lambda_{NPAMF}$, and $\Lambda_{LRNAMF}$ as functions of $RB$s, $SNR$s, and sample support, a portion ($J = 2$, $N = 32$, and $RB = 1000$) of the clutter-only datacube is processed. However, the allowed CUTs are in the range of $(K/2) + 1$ to $1000 - (K/2)$. For Figure 1, We selected the CUT to be from 475 to 525. The cutoff $SNR$s are then determined at the condition when those three $\Lambda$s at $RB = 493$, 500, and 507 are greater than the rest of $\Lambda$s at other $RB$s. In the simulation, the model order of the NPAMF is chosen to be $P = 4$ and the clutter rank for the LRNAMF is $r = 42$. For array elements $J = 2$, and pulses $N = 32$, since the sample matrix inversion in the NAMF method becomes ill-conditioned when $K \leq 64$, the cutoff $SNR$s for NAMF are only available for $K > 64$, which is the curve with '+' symbol in Figure 1. When the sample support is in the range, $K < 2JN = 128$), the LRNAMF has smaller cutoff $SNR$ than the NAMF and NPAMF. In the range that $72 \leq K \leq 3JN = 192$, the cutoff $SNR$ for the NAMF is always smaller than that of the NPAMF except at $K = 128$, where these three algorithms have the same cutoff $SNR$. When $128 \leq K \leq 192$, the LRNAMF has the larger cutoff $SNR$s than the NAMF and NPAMF but the difference of all cutoff $SNR$s is less than 3dB. In the next section, we will demonstrate that to provide a good detection performance, the LRNAMF requires a small sample support, $K_{LRNAMF} = 2r = 84$ and has less computational complexity than NAMF and NPAMF. Hence, this study illustrates that LRNAMF out-performs NPAMF and NAMF for the KASSPER L-band datacube as long as there are few outliers in the training data. Note that at small sample support, the cutoff $SNR$ for the NPAMF and LRNAMF rise rapidly as shown in Figure 1. This is attributed to the fact that the sample support is too small to yield a good estimate of the disturbance covariance matrices for LRNAMF or to compute $P$th-order multichannel linear autoregressive coefficients for NPAMF) appropriately. Furthermore, at very small sample support, i.e., $K < 16$, NPAMF requires the cutoff $SNR$ be greater than 0dB in order to be able to detect these three targets simultaneously.

| Parameter | Value |
|---|---|
| Carrier frequency | 1240 MHz |
| Bandwidth | 10 MHz |
| Number of antenna elements ($J$) | 11 |
| Number of pulses ($N$) | 32 |
| Pulse repetition frequency ($T^{-1}$) | 1984 Hz |
| interelement spacing ($d$) | 0.1092 m |
| 1000 range bins | 35 km to 50 km |
| 91 azimuth angles ($AZ$) | $87^o$,$89^o$,...$267^o$ |
| 128 Doppler beam position ($DBP$) | -0.5 to 0.5 |
| Clutter-to-noise ratio ($CNR$) | 40dB |
| Platform speed | 100 m/s |

**Table 1**. KASSPER L-band datacube parameters

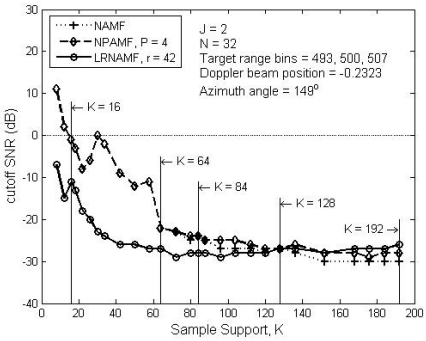


**Fig. 1**. Cutoff signal-to-noise ratio versus sample supports

## 3. TARGET CANCELLATION EFFECT AND STEERING VECTOR MATCHED AND MISMATCHED CASES

In this section, NAMF, NPAMF, and LRNAMF are applied to compute test statistics versus range bins ($RB$s) and filter outputs versus azimuth angles ($AZ$) and Doppler beam position ($DBP$) for two situations when the steering vectors for manually inserted targets are either known or unknown. The outlier-free training data are selected from the clutter-only datacube, which is generated from true clutter covariance matrices for the KASSPER L-band radar clutter. On the other hand, the outlier contaminated training data are selected from the primary datacube, in which three targets are manually inserted to the clutter-only datacube at $RB = 493$, 500, and 507. In other words, these manually inserted targets also serve as outliers in the outlier-contaminated training data. All three inserted targets are assumed to have identical $DBP = -0.2323$, $AZ = 149^o$, and $SNR = 40$dB. Other system parameters used for the simulations in this section are fixed at $J = 11$ and $N = 32$ so that the spatio-temporal product, $JN$, is equal to 352.

The sample support $K$ for each algorithm is also specified in each figure as well as the model order $P$ for the NPAMF and the clutter rank $r$ for the LRNAMF. For most

simulations, we select the following parameters, $K_{NAMF} = 704$, $K_{NPAMF} = 16$, $K_{LRNAMF} = 84$, $P = 4$, and $r = 42$. Occasionally, we also highlight the value of $K_{NPAMF}$ in the caption of the figure for the purpose of illustrating the improved detection performance of the NPAMF when $K_{NPAMF}$ is increased to 352. Again the sliding window processing (SWP) are adopted for all simulations and the training data are selected equally from both sides of the CUT. To expedite the computation, the range of CUTs are chosen from 485 to 515.

Case 1: Known Steering Vector

In this case, disturbance covariance matrices, $\hat{\mathbf{R}}_d$, for all CUTs are estimated for two possible situations: (1) training data are outlier-free and (2) training data are contaminated with outliers. The test statistics for the NAMF, NPAMF, and LRNAMF, namely, $\Lambda_{NAMF}$, $\Lambda_{NPAMF}$, and $\Lambda_{LNRAMF}$, are computed from Eqs. (3) to (5), in which the spatio-temporal steering vector, **e**, is selected from all "look" steering vectors. The $DBP$s and $AZ$s for "look" steering vectors will be designated as $DBP_L$s and $AZ_L$s. We select 128 $DBP_L$s having the range from -0.5 to 0.5 and 91 $AZ_L$s from $87^o$ to $267^o$ as shown in Table 1. To compute the test statistics, three targets are manually inserted into the primary data, **x**, at $RB = 493$, 500, and 507 as well as at $DBP_L = DBP_T = -0.2323$ and $AZ_L = AZ_T = 149^o$. Thus, the target steering vector will only match with one of the "look" steering vectors. For the following simulations, the $SNR$ is fixed at 40dB. Then, we compute the test statistics for the NAMF, NPAMF, and LRNAMF as given in Eqs. (3) to (5) as functions of $RB$s, $DBP_L$s, and $AZ_L$s. The legend either "no" or "yes" in the following figures indicates that the training data used for estimating the disturbance covariance matrices are either outlier-free or contaminated with outliers.

We illustrate the azimuth-angle mismatch in Figure 2 where $DBP_L = DBP_T = -0.2323$ and $AZ_L = 147^o < AZ_T = 149^o$ as well as the Doppler-beam-position mismatch in Figure 3 where $AZ_L = AZ_T = 149^o$ but $DBP_L = -0.2402 < DBP_T = -0.2323$. It indicates that when the target steering vector is known, test statistics obtained from simulations are very sensitive to the misalignment of the "look" steering vector with respect to the target steering vector so that the target cannot be detected regardless whether the training data contain outliers or not. Only when the "look" steering vector matches perfectly with that of the desired target, these three targets at $RB = 493$, 500, and 507 can be detected from the application of NAMF and LRNAMF algorithms as shown in Figure 4. Since sample support for the NAMF and LRNAMF, $K_{NAMF} = 704 = 2JN$ and $K_{LRNAMF} = 84 = 2r$, satisfy the RMB rule, both of them have better performance than the NPAMF with small sample support $K_{NPAMF}$. This is because at small sample

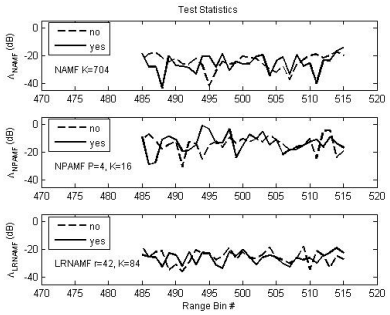


**Fig. 2**. Angular mismatched case when $AZ_L = 147^o$

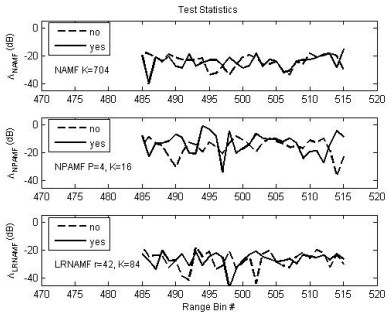


**Fig. 3**. Doppler mismatched case at $DBP_L = -0.2402$

support, $K_{NPAMF} = 16$, and with the presence of outliers in the training data, the computed $P$th-order multichannel linear autoregressive coefficients are insufficient to whiten the spatio-temporal data vector and subsequently lead to worse detection performance for the NPAMF. In fact, from other investigations, it also indicates that if $K_{NAMF} < 2JN$ and $K_{LRNAMF} < 2r$, the detection performance of both NAMF and LRNAMF is also deteriorated in the same manner as that of the NPAMF.

After a series of computations by varying $K_{NPAMF}$ from 8 to 704, we observed that the NPAMF with $K_{NPAMF} = 352$ can yield equivalent performance to the NAMF and LRNAMF with $K_{NAMF} = 704$ and $K_{LRNAMF} = 84$, respectively, as shown in Figure 5. This observation confirms that for the KASSPER L-band datacube, the LRNAMF can

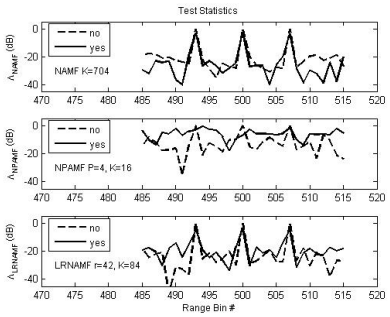


**Fig. 4**. Angular and Doppler matched case

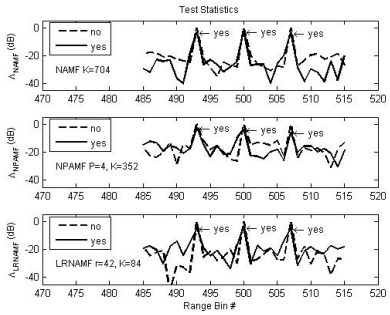


**Fig. 5**. Angular and Doppler matched case when $K_{NPAMF} = 352$

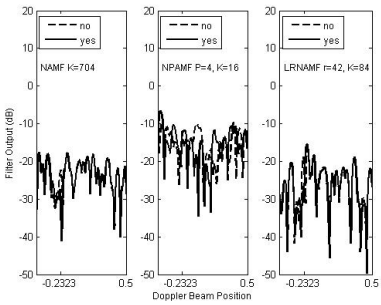


**Fig. 6**. Angular mismatched case at $RB = 493$ when $AZ_L = 147^o$

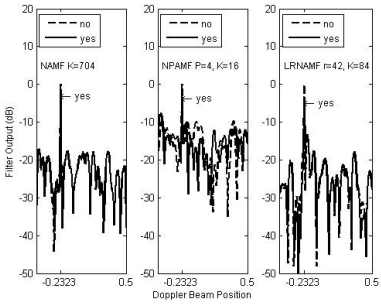


**Fig. 7**. Angular matched case at $RB = 493$

provide better detection performance with less computational complexity than NAMF and NPAMF. The target cancellation effect (as indicated by the symbol "← yes" that points to the peak of the solid curve in Figure 5) is also illustrated for all three algorithms, where it shows that at three "true" target range bins, those $\Lambda$ values of the solid curve (computed for the outlier-contaminated case) are always less than those of the dashed curve (computed for the outlier-free case).

At the desired range bin, $RB = 493$, filter outputs for NAMF, NPAMF, and LRNAMF versus $DBP$ and $AZ$ are plotted in Figures 6 to 9 to demonstrate the angular and Doppler mismatched and matched cases. It is shown in Figures 6 and 8 that the target cannot be detected when there is a slight mismatch between $DBP_L$ (and/or $AZ_L$) and $DBP_T$ (and/or $AZ_T$). Only when there is a perfect match between both values of $DBP_L$ and $AZ_L$) with that of $DBP_T$ and $AZ_T$), a sharp detection peak in the filter outputs can then be observed at correct $DBP_T$ and $AZ_T$ for the desired target as shown in Figures 7 and 9. Also, the target cancellation effect can be observed (as indicated by the symbol "← yes" that points to the peak of the solid curve) in these two Figures 7 and 9.

For target detection, various threshold settings are applied to the test statistics in order to determine the detection performance of the NAMF, NPAMF, and LRNAMF. In Figures 10 to 12, we present three threshold settings used by these three algorithms to detect targets under the condition that the training data are free of outliers. The "true" locations for three inserted targets are specified by the "x" symbols while the detected locations by the "o" symbols. It is shown that when the training data are free of outliers and when the threshold setting is optimal, all three algorithms can correctly detect the "true" locations of these three targets provided that the target $SNR$ is greater than -30dB, which is also implied in Figure 1. On the contrary, if the training data are contaminated with outliers and if the sample support is small, e.g., $K_{NPAMF} = 16$), there is no suitable threshold for the NPAMF to detect all three targets simultaneously. This is shown in Figure 13, where even a very low threshold at -20dB is chosen, the NPAMF can only detect two targets but yields many false alarms at the same time. It turns out that when $K_{NPAMF}$ is increased to 352, then the NPAMF has the equivalent detection performance as NAMF and LRNAMF with $K_{NAMF} = 704$ and $K_{LRNAMF} = 84$, respectively. This is illustrated in Figure 14 with a maximum threshold for optimal detection at $K_{NPAMF} = 352$.

Case 2: Steering Vector Uncertainty

The disturbance covariance matrices, $\hat{\mathbf{R}}_d$, for all CUTs and the test statistics, $\Lambda_{NAMF}$, $\Lambda_{NPAMF}$, and $\Lambda_{LNRAMF}$,

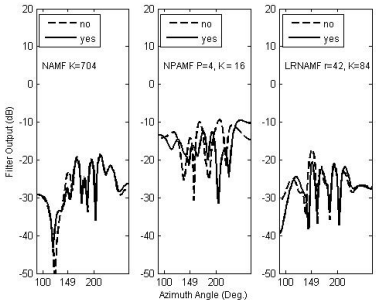


**Fig. 8**. Doppler mismatched case at $RB = 493$ and $DBP_L = -0.2402$

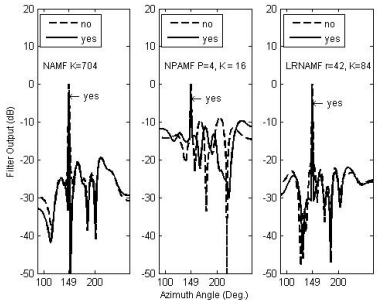


**Fig. 9**. Doppler matched case at $RB = 493$

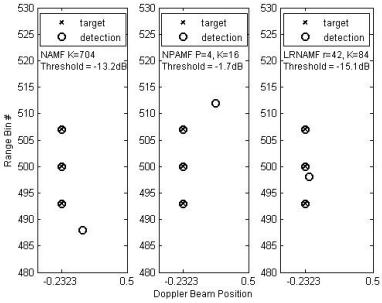


**Fig. 10**. Target detection with low thresholds for outlier-free training data

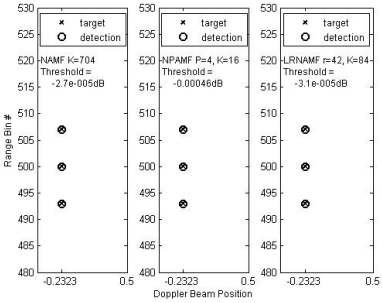


**Fig. 11**. Optimal target detection with maximum thresholds for outlier-free training data

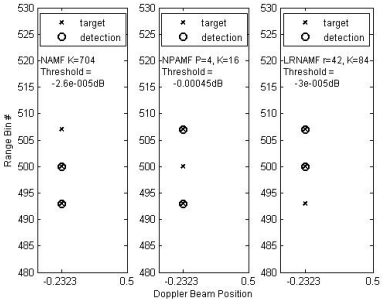


**Fig. 12**. Target detection with high thresholds for outlier-free training data

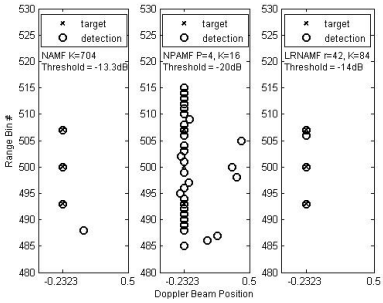


**Fig. 13**. Target detection with Low thresholds for outlier-contaminated training data

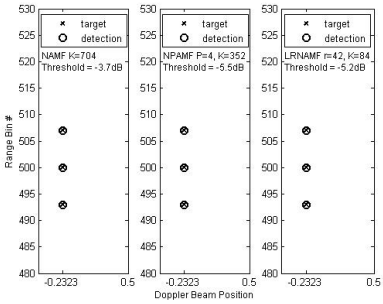


**Fig. 14**. Optimal target detection with maximum thresholds for outlier-contaminated training data at $K_{NPAMF} = 352$

are computed also for two situations: (1) training data are outlier-free and (2) training data are contaminated with outliers. Since there is an uncertainty in the spatio-temporal steering vector of the desired target, during the computation of the test statistics, these targets are manually inserted into the primary data, **x**, at correct $RB = 493$, 500, and 507 but without specifying the condition that $DBP_L = DBP_T = -0.2323$ and $AZ_L = AZ_T = 149^o$. In this case, the simulation can't guarantee that the target steering vector will only match with one of the "look" steering vectors. The test statistics are shown in Figures 15 to 18. In Figures 15 and 16, we show that when the training data are outlier-free, targets at $RB = 493$, 500, and 507 can be detected with incorrect "look" steering vector if either $AZ_L$ or $DBP_L$ is slightly different than $AZ_T$ or $DBP_T$. In fact, within the range that $-0.2638 < DBP_L < -0.2008$ and $135^o < AZ_L < 161^o$, those three targets can be detected even though $DBP_L$ and $AZ_L$ are different from $DBP_T$ and $AZ_T$. In addition, with the outlier-free training data, the target detection performance for this case is the same as the case with known steering vector as shown in Figures 10 to 12. At the desired range bin, $RB = 493$, Figures 19 to 22 illustrate that if the training data are free of outliers and if there is a slight mismatch between $DBP_L$ (and/or $AZ_L$) and $DBP_T$ (and/or $AZ_T$), there is a substantial broadening of detection peak at $DBP_L = -0.2323$ or at $AZ_L = 149^o$.

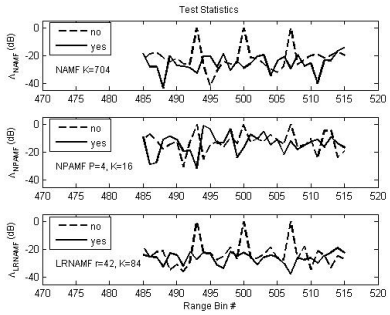


**Fig. 15**. Angular mismatched case when $AZ_L = 147^o$

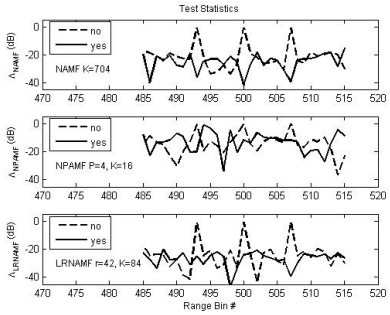


**Fig. 16**. Doppler mismatched case when $DBP_L = -0.2402$

This broadening causes false alarms as if a target were detected by the incorrect "look" steering vector as shown in dashed curves of Figures 19 and 21. On the contrary, if the training data is contaminated by outliers having identical steering vector and if there is a slight mismatch between the "look" steering vector and the target, there is no detection as shown in solid curves of Figures 19 and 21. Only when there is a perfect match between the "look" steering vector and the target, there is a sharp detection peak in the filter output at the correct $DBP_L = DBP_T = -0.2323$ and $AZ_L = AZ_T = 149^o$ as shown in Figures 20 and 22. Moreover, in Figures 20 and 22, the target cancellation effect can be observed (as indicated by the symbol "← yes" that points to the detection peak on the solid curve).

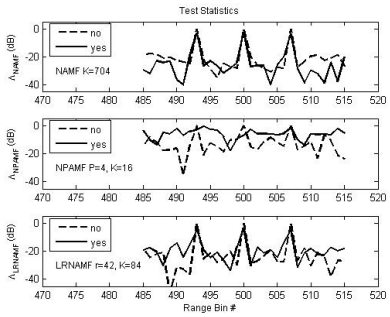


**Fig. 17**. Angular and Doppler matched case

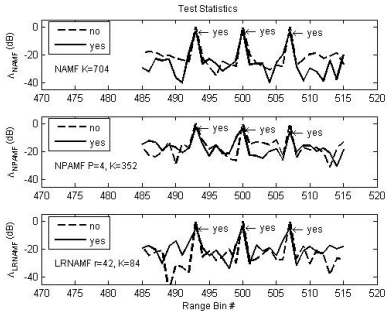


**Fig. 18**. Angular and Doppler matched case when $K_{NPAMF} = 352$

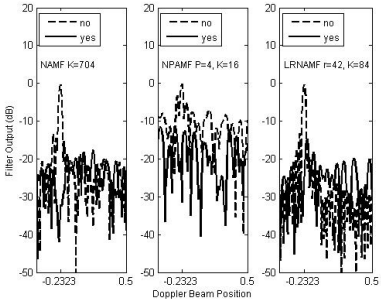


**Fig. 19**. Angular mismatched case at $RB = 493$ and $AZ_L = 147^o$

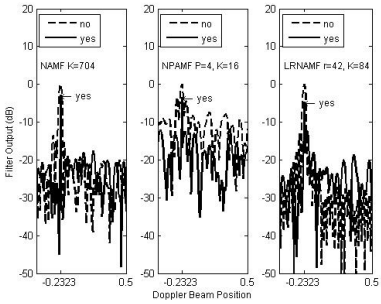


**Fig. 20**. Angular matched case at $RB = 493$

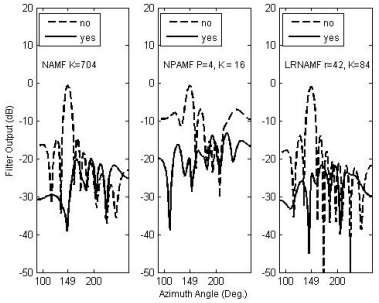


**Fig. 21**. Doppler mismatched case at $RB = 493$ and $DBP_L = -0.2402$

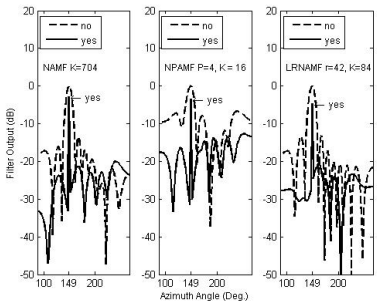


**Fig. 22**. Doppler matched case at $RB = 493$

## 4. SUMMARY

In this paper, we showed that when the signal-to-noise ratio ($SNR$) is used as a target-detection parameter, the LRNAMF can outperform NAMF and NPAMF if the sample support $K$ for all three algorithms are within the RMB rule, i.e., $K \leq 2JN$. In other words, the LRNAMF requires less sample support and can detect targets with smaller $SNR$ than NAMF and NPAMF. Second, we have demonstrated that when the training data are contaminated with outliers, the target cancellation effect is revealed in diminished filter outputs for all three algorithms. In the known steering vector case, if the training data are free of outliers, there is a wider range of threshold settings for these three algorithms to choose in order to detect targets without causing false alarms. Finally, we present a realistic and problematic scenario for target detection in heterogenous radar clutter environment. Namely, when there is uncertainty in the spatio-temporal steering vector, the detection peak in the filter output is substantially broadened for all three algorithms. The broadening in the filter output introduces false alarms attributed to the ambiguity of determining correct $DBP_T$ and $AZ_T$ for each individual target.

## 5. REFERENCES

[1] L. E. Brennan and I. S. Reed. Theory of adaptive radar. *IEEE Trans. on Aerospace and Electronic Systems*, **AES-9**:237–252, 1973.

[2] R. Klemm. Adaptive clutter suppression for airborne phased array radars. *IEE Proceedings*, **130**, Pts. F and H, 1:125–131, 1983.

[3] E.C. Barile, R.L. Fante, and J.A. Torres. Some limitations on the effectiveness of airborne adaptive radar. *IEEE Trans. on Aerospace and Electronic Systems*, **AES-28**:1015–1032, 1992.

[4] H. Wang and L. Cai. On adaptive spatial-temporal processing for airborne surveillance radar systems. *IEEE Trans. on Aerospace and Electronic Systems*, **30**, 3:660–669, 1994.

[5] J. Ward. Space-time adaptive processing for airborne radar. Technical Report Technical Report 1015, ," MIT Lincoln Laboratory, December 1994.

[6] I.S. Reed, J.D. Mallett, and L.E. Brennan. Rapid convergence rate in adaptive arrays. *IEEE Trans. on Aerospace and Electronic Systems*, **AES-10**:853–863, 1974.

[7] I.P. Kirsteins and D.W. Tufts. Adaptive detection using a low rank approximation to a data matrix. *IEEE Trans. on Aerospace and Electronic Systems*, **AES-30**:55–67, 1994.

[8] M. J. Steiner and K.R. Gerlach. Fast converging adaptive processor for a structured covariance matrix. *IEEE Trans. on Aerospace and Electronic Systems*, **36**, no.4:1115–1126, 2000.

[9] J.R. Roman, M. Rangaswamy, D.W. Davis, Q. Zhang, B.Himed, and J.H. Michels. Parametric adaptive matched filter for airborne radar applications. *IEEE Trans. on Aerospace and Electronic Systems*, **36**, no.2:677–692, 2000.

[10] M. Rangaswamy. Normalized Matched Filter-A Low Rank Approach. In *36th Asilomar Conference on Signals, Systems, and Computers*, Pacific Grove, CA, November 3-6, 2002.

[11] M. Rangaswamy, F.C. Lin, and K. Gerlach. Robust adaptive signal processing methods for heterogeneous radar clutter scenario. *special issue of the EURASIP J. Signal Processing: New Trends and Findings in Antenna Array Processing for Radar*, **84**:1653–1665, 2004.

[12] Shawn Kraut, Louis L. Scharf, and L.T. McWhorter. Adaptive subspace detectors. *IEEE Trans. on Signal Processing*, **49**:1–16, 2001.

[13] J.H. Michels, M. Rangaswamy, and B. Himed. Performance of parametric and covariance based STAP tests in Compound-Gaussian Clutter. *Digital Signal Processing*, 12, nos.2,3:307–328, 2002.

[14] J.S. Bergin and P.M. Techau. High-fidelity site-specific radar simulation: Kassper'02 workshop datacube. Technical Report ISL-SCRD-TR-02-105, Defense Advanced Research Projects Agency, 2002.